Title
Nematic Fluctuations in the Non-Superconducting Iron Pnictide BaFe1.9−x Ni0.1Cr x As2

Authors
Gong, Dongliang
Yi, Ming
Wang, Meng
et al.

Publication Date
2022

DOI
10.3389/fphy.2022.886459

Peer reviewed

frontiers

Author's Proof

Before checking your proof, please see the instructions below.

- Carefully read the entire proof and mark all corrections in the appropriate place, using the Adobe Reader commenting tools (**Adobe Help**).
- Provide your corrections in a single PDF file or post your comments in the Production forum making sure to reference the relevant query/line number. Upload or post all your corrections directly in the Production Forum to avoid any comments being missed.
- We do not accept corrections in the form of edited manuscripts nor via email.
- Do not provide scanned or handwritten corrections.
- Before you submit your corrections, please make sure that you have checked your proof carefully as once you approve it, you won't be able to make any further corrections.
- To ensure the timely publication of your article, please submit the corrections within 48 hours. After submitting, do not email or query asking for confirmation of receipt.

Do you need help? Visit our **Production Help Center** for more information. If you can't find an answer to your question, contact your Production team directly by posting in the Production Forum.

Quick Check-List

- ☐ **Author names** - Complete, accurate and consistent with your previous publications
- ☐ **Affiliations** - Complete and accurate. Follow this style when applicable: Department, Institute, University, City, Country
- ☐ **Tables** - Make sure our formatting style did not change the meaning/alignment of your Tables.
- ☐ **Figures** - Make sure we are using the latest versions.
- ☐ **Funding and Acknowledgments** - List all relevant funders and acknowledgments.
- ☐ **Conflict of Interest** - Ensure any relevant conflicts are declared.
- ☐ **Supplementary files** - Ensure the latest files are published and that no line numbers and tracked changes are visible. Also, the supplementary files should be cited in the article body text.
- ☐ **Queries** - Reply to all typesetters queries below
- ☐ **Content** - Read all content carefully and ensure any necessary corrections are made.

frontiers | Frontiers in Physics

ORIGINAL RESEARCH
published: XX XX 2022
doi: 10.3389/fphy.2022.886459

Nematic Fluctuations in the Non-Superconducting Iron Pnictide $BaFe_{1.9-x}Ni_{0.1}Cr_xAs_2$

Dongliang Gong[1,2†], *Ming Yi*[3,4], *Meng Wang*[5], *Tao Xie*[1,2†], *Wenliang Zhang*[1,2†], *Sergey Danilkin*[6], *Guochu Deng*[6], *Xinzhi Liu*[5], *Jitae T. Park*[7], *Kazuhiko Ikeuchi*[8], *Kazuya Kamazawa*[8], *Sung-Kwan Mo*[9], *Makoto Hashimoto*[10], *Donghui Lu*[10], *Rui Zhang*[11], *Pengcheng Dai*[11], *Robert J. Birgeneau*[4,12,13], *Shiliang Li*[1,2,14] *and Huiqian Luo*[1,14]*

[1]*Beijing National Laboratory for Condensed Matter Physics, Institute of Physics, Chinese Academy of Sciences, Beijing, China,* [2]*School of Physical Sciences, University of Chinese Academy of Sciences, Beijing, China,* [3]*Department of Physics and Astronomy, Rice University, Houston, TX, United States,* [4]*Department of Physics, University of California, Berkeley, Berkeley, CA, United States,* [5]*School of Physics, Sun Yat-Sen University, Guangzhou, China,* [6]*Australian Centre for Neutron Scattering, Australian Nuclear Science and Technology Organisation, Lucas Heights, NSW, Australia,* [7]*Heinz Maier-Leibnitz Zentrum (MLZ), Technische Universität München, Garching, Germany,* [8]*Neutron Science and Technology Center, Comprehensive Research Organization for Science and Society, Tokai, Japan,* [9]*Lawrence Berkeley National Laboratory, Berkeley, CA, United States,* [10]*Stanford Synchrotron Radiation Lightsource, SLAC National Accelerator Laboratory, Menlo Park, CA, United States,* [11]*Department of Physics and Astronomy, Rice Center for Quantum Materials, Rice University, Houston, TX, United States,* [12]*Materials Science Division, Lawrence Berkeley National Laboratory, Berkeley, CA, United States,* [13]*Department of Materials Science and Engineering, University of California, Berkeley, Berkeley, CA, United States,* [14]*Songshan Lake Materials Laboratory, Dongguan, China*

The main driven force of the electronic nematic phase in iron-based superconductors is still under debate. Here, we report a comprehensive study on the nematic fluctuations in a non-superconducting iron pnictide system $BaFe_{1.9-x}Ni_{0.1}Cr_xAs_2$ by electronic transport, angle-resolved photoemission spectroscopy (ARPES), and inelastic neutron scattering (INS) measurements. Previous neutron diffraction and transport measurements suggested that the collinear antiferromagnetism persists to $x = 0.8$, with similar Néel temperature T_N and structural transition temperature T_s around 32 K, but the charge carriers change from electron type to hole type around $x = 0.5$. In this study, we have found that the in-plane resistivity anisotropy also highly depends on the Cr dopings and the type of charge carriers. While ARPES measurements suggest possibly weak orbital anisotropy onset near T_s for both $x = 0.05$ and $x = 0.5$ compounds, INS experiments reveal clearly different onset temperatures of low-energy spin excitation anisotropy, which is likely related to the energy scale of spin nematicity. These results suggest that the interplay between the local spins on Fe atoms and the itinerant electrons on Fermi surfaces is crucial to the nematic fluctuations of iron pnictides, where the orbital degree of freedom may behave differently from the spin degree of freedom, and the transport properties are intimately related to the spin dynamics.

Keywords: iron-based superconductors, electronic nematic phase, nematic fluctuations, resistivity, spin excitations, orbital ordering, neutron scattering

OPEN ACCESS

Edited by:
Ivar Martin,
Argonne National Laboratory (DOE), United States

Reviewed by:
Andreas Kreisel,
Leipzig University, Germany
Yao Shen,
Brookhaven National Laboratory (DOE), United States

***Correspondence:**
Huiqian Luo
hqluo@iphy.ac.cn

†Present addresses:
Dongliang Gong,
Department of Physics and Astronomy, University of Tennessee, Knoxville TN 37996, United States
Tao Xie,
Neutron Scattering Division, Oak Ridge National Laboratory, Oak Ridge, Tennessee 37831, United States
Wenliang Zhang,
Photon Science Division, Swiss Light Source, Paul Scherrer Institut, CH-5232 Villigen PSI, Switzerland

Specialty section:
This article was submitted to Condensed Matter Physics, a section of the journal Frontiers in Physics

Received: *28 February 2022*
Accepted: *12 April 2022*
Published: *XX XX 2022*

Citation:
Gong D, Yi M, Wang M, Xie T, Zhang W, Danilkin S, Deng G, Liu X, Park JT, Ikeuchi K, Kamazawa K, Mo S-K Hashimoto M, Lu D, Zhang R, Dai P, Birgeneau RJ, Li S and Luo H (2022) Nematic Fluctuations in the Non-Superconducting Iron Pnictide $BaFe_{1.9-x}Ni_{0.1}Cr_xAs_2$. Front. Phys. 10:886459. doi: 10.3389/fphy.2022.886459

1 INTRODUCTION

Electronic nematic phase breaks the rotational symmetry but preserves the translational symmetry of the underlying lattice in correlated materials [1–4]. In iron-based superconductors, the nematic order associated with a tetragonal-to-orthorhombic structural transition at temperature T_s acts as a precursor of the magnetic order below T_N and the superconducting state below T_c [5–10]. The nematic fluctuations can be described by the electronic nematic susceptibility, which is defined as the susceptibility of electronic anisotropy to the uniaxial in-plane strain [11]. Divergent nematic susceptibility upon approaching T_s from high temperature is revealed by the elastoresistance and elastic moduli measurements, suggesting nematic fluctuations well above T_s [12–16]. The nematic fluctuations commonly exist in iron-based superconductors and are even present in compounds with tetragonal crystal symmetry without any static nematic order [17]. Accumulating evidence suggests that the optimal superconductivity with maximum T_c usually occurs near a nematic quantum critical point where the nematic fluctuations are the strongest [18–29]. However, the charge, spin, and orbital degrees of freedom are always intertwined in the presence of nematic fluctuations [30–39], giving a twofold rotational (C_2) symmetry in many physical properties [5–11, 40–44] including anisotropic in-plane electronic resistivity and optical conductivity [45–51], lifting of degeneracy between d_{xz}/d_{yz} orbitals [52–58], anisotropic spin excitations at low energies [59–63], phonon-energy split in lattice dynamics [64, 65], and splitting of the Knight shift [66, 67]. In addition, it has been proposed that the local anisotropic impurity scattering of chemical dopants likely induces the twofold symmetry in the transport properties [68–70]. Such complex cases make it is difficult to clarify the main driven force of nematic phase by a single experimental probe.

Our previous works suggest that the Cr substitution is an effective way both to suppress the superconductivity and to tune the magnetism in iron-based superconductors [27, 71–73]. Specifically, in the $BaFe_{1.9-x}Ni_{0.1}Cr_xAs_2$ system, by continuously doping Cr to the optimally superconducting compound $BaFe_{1.9}Ni_{0.1}As_2$ with T_c = 20 K, the superconductivity is quickly suppressed above x = 0.05, but the magnetic transition temperature T_N and the structural transition temperature T_s remain between 30 and 35 K as shown by neutron diffraction results on naturally twinned samples (**Figure 1A**). Moreover, the effective moment m is significantly enhanced first and then suppressed for dopings higher than x = 0.5, where the charge carriers change from electron type to hole type as shown by the sign of Hall and Seebeck coefficients [73]. These make $BaFe_{1.9-x}Ni_{0.1}Cr_xAs_2$ a rare example to separately tune the magnetically ordered temperature T_N by the local spin interactions and the magnetically ordered strength by the scattering of itinerant electrons on Fermi surfaces, respectively. The extra holes introduced by Cr substitutions compensate the electron doping thus may drive those non-superconducting compounds to a half-filled Mott insulator similar to the parent compounds of cuprate and nickelate superconductors [74–79]. It would be interesting to monitor the evolution of the nematic fluctuations starting from a metallic state toward to a localized insulating state [79–81], especially on the detwinned samples (**Figure 1B**).

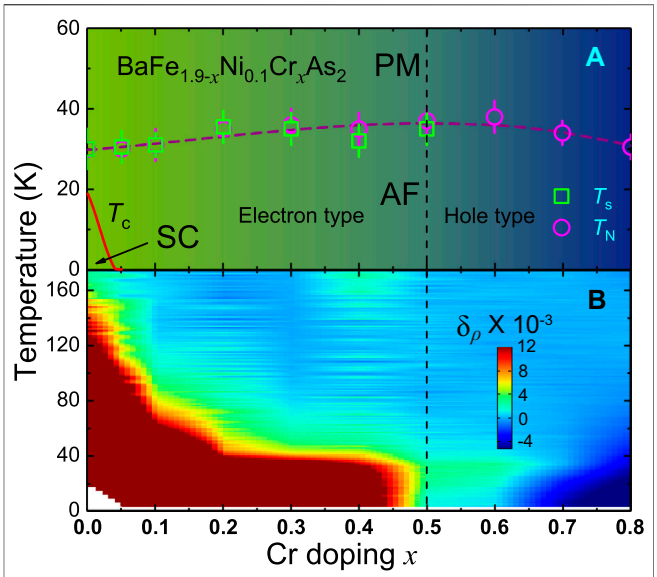

FIGURE 1 | (Color online) Phase diagram and in-plane resistivity anisotropy of $BaFe_{1.9-x}Ni_{0.1}Cr_xAs_2$. **(A)** The PM, AF, and SC mark the region of paramagnetic, antiferromagnetic, and superconducting phases defined by T_s, T_N, and T_c, respectively. Here, T_s and T_N were measured by neutron diffraction in our previous work on the naturally twinned samples [73]. **(B)** The gradient color maps the in-plane resistivity anisotropy δ_ρ measured on detwinned samples. The vertical dashed line divides the regions for electron-type and hole-type charge carriers as determined by the sign of Hall and Seebeck coefficients [73].

In this paper, we further report a multi-probe study on the nematic fluctuations in the non-superconducting compounds $BaFe_{1.9-x}Ni_{0.1}Cr_xAs_2$ (x = 0.05 ~ 0.8) by electronic transport, angle-resolved photoemission spectroscopy (ARPES), and inelastic neutron scattering (INS) measurements. The in-plane resistivity anisotropy measured in the detwinned samples under uniaxial pressure shows a strong dependence on the Cr content with a clear sign change above x = 0.6. By focusing on two compounds with x = 0.05 and 0.5, ARPES measurements suggest possible band shifts induced by orbital anisotropy near T_s/T_N for both dopings, but INS experiments reveal clearly different behaviors on the spin nematicity. The onset temperature of low-energy spin excitation anisotropy between Q = (1, 0, 1) and Q = (0, 1, 1) for x = 0.05 is about 110 K, but for x = 0.5, it is much lower, only about 35 K near the magnetic transition. Such temperature dependence of spin nematicity is consistent with the results of in-plane resistivity anisotropy. At high energies, the spin nematicity for x = 0.05 extends to about 120 meV, much larger than the case for x = 0.5 (about 40 meV), suggesting a possible linear correlation between the highest energy scale and the onset temperature of spin nematicity. Therefore, the nematic behaviors in iron pnictides are highly related to the interplay between local moments and itinerant electrons. While the C_2-type anisotropies in spin excitations and

in-plane resistivity are strongly correlated with each other [60], the orbital anisotropy induced band splitting may behave differently as affected by the complex Fermi surface topology [82–91].

2 EXPERIMENT DETAILS

High-quality single crystals of $BaFe_{1.9-x}Ni_{0.1}Cr_xAs_2$ were grown by the self-flux method [71–73, 92–95]; the characterization results of our sample can be found in previous reports [71, 73]. The crystalline directions of our sample were determined by an X-ray Laue camera (*Photonic Sciences*) in the backscattering mode with incident beam along the c − axis. After that, the crystals were cut into rectangle shapes (typical sizes: 1 mm × 2 mm) by a wire saw under the directions [1, 0, 0] × [0, 1, 0] in orthorhombic lattice notation ($a = b = 5.6$ Å). By applying a uniaxial pressure around 10 MPa, the crystal can be fully detwinned at low temperature, where the direction of pressure was defined as the b direction, and the pressure-free direction was defined as the a direction [60–63, 96–99]. The in-plane resistivity ($\rho_{a,b}$) was measured by the standard four-probe method with the Physical Property Measurement System (PPMS) from Quantum Design. To compare the temperature dependence of resistivity at different directions, we normalized the resistivity $\rho_{a,b}(T)$ data at 150 K for each sample. The in-plane resistivity anisotropy was defined by $\delta_\rho = (\rho_b - \rho_a)/(\rho_b + \rho_a)$ same as other literature [45–47].

ARPES experiments were performed at beamline 10.0.1 of the Advanced Light Source and beamline 5-4 of the Stanford Synchrotron Radiation Light source with R4000 electron analyzers. The angular resolution was 0.3°, and the total energy resolution was 15 meV. All samples were cleaved *in-situ* at 10 K and measured in ultra-high vacuum with a base pressure lower than 4×10^{-11} Torr. We note that we used twinned samples without uniaxial pressure for the ARPES experiments. INS experiments were carried out at two thermal triple-axis spectrometers: PUMA at Heinz Maier-Leibnitz Zentrum (MLZ) [100], Germany, and TAIPAN at the Australian Centre for Neutron Scattering (ACNS) [101], ANSTO, Australia. The wave vector **Q** at (q_x, q_y, q_z) was defined as (H, K, L) = ($q_x a/2\pi$, $q_y b/2\pi$, $q_z c/2\pi$) in reciprocal lattice units (r.l.u.) using the orthorhombic lattice parameters $a \approx b = 5.6$ Å and $c \approx 13$ Å. All measurements were done with fixed final energy $E_f = 14.8$ meV, and a double focusing monochromator and analyzer using pyrolytic graphite crystals. To gain a better signal-noise ratio, eight pieces of rectangularly cut crystals (typical sizes: 7 mm × 8 mm × 0.5 mm) were assembled in a detwinned device made by aluminum and springy gaskets [60–63]. To reach both Q = (1, 0, 1) and Q = (0, 1, 1), the sample holder was designed to easily rotate by 90°, thus the scattering plane can switch from [H, 0, 0] × [0, 0, L] to [0, K, 0] × [0, 0, L]. The total mass of the crystals used in INS experiments was about 2 g from each sample set of $x = 0.05$ and $x = 0.5$. Time-of-flight neutron scattering experiments were carried out on the same sample sets at 4SEASONS spectrometer (BL-01) at J-PARC [102, 103], Tokai, Japan, with multiple incident energies E_i = 250, 73, 34, 20 meV, k_i parallel to the c axis, and chopper frequency f = 250 Hz. The data were only corrected by the efficiency of detectors from the incoherent scattering of vanadium with white beam. As we were comparing two samples with similar mass under the same measured conditions at the same spectrometer, it was not necessary to do the vanadium normalization with mono-beam. The data were analyzed by the Utsusemi and MSlice software packages [104, 105].

3 RESULTS AND DISCUSSIONS

We first present the resistivity results in **Figures 1**-**3**. Apparently, the in-plane resistivity anisotropy show a strong dependence on the Cr doping level. In the Cr free sample $BaFe_{1.9}Ni_{0.1}As_2$, the difference between ρ_a and ρ_b presents above the superconducting transition temperature $T_c = 20$ K, where ρ_a is metallic and ρ_b is semiconducting-like with an upturn at low temperature (namely, $\rho_a < \rho_b$) (**Figure 2A**). The superconductivity is completely suppressed at $x = 0.05$, and there is a dramatic difference between ρ_a and ρ_b with an anisotropy δ_ρ persisting to about $T = 110$ K (**Figure 2B**). By further increasing Cr doping, both ρ_a and ρ_b become semiconducting-like even insulating-like above $x = 0.1$, and the resistivity anisotropy gets weaker and weaker, until it nearly disappears at $x = 0.5$ and 0.6 compounds (**Figure 2C–H**). For those high doping compounds $x = 0.7$ and 0.8, it seems that δ_ρ changes sign with $\rho_a > \rho_b$ at low temperatures (**Figure 2I,J**). To clearly compare the resistivity anisotropy upon Cr doping, we plot δ_ρ as gradient color mapping in **Figure 1B** and show its detailed temperature dependence in **Figure 3**. Interestingly, the sign of δ_ρ is also related to the type of charge carriers. δ_ρ keeps strong and positive in the electron-type compounds but changes to negative and weak ($< 1\%$) in the hole-type compounds (**Figure 1B** and **Figure 3B**). This is consistent with the results in the electron doped $BaFe_{2-x}(Ni, Co)_xAs_2$ and the hole doped $Ba_{1-x}K_xFe_2As_2$, $Ca_{1-x}Na_xFe_2As_2$, and $BaFe_{2-x}Cr_xAs_2$ systems [45–48, 106–109]. However, in those cases, the onset temperature of δ_ρ decreases with the structural transition temperature T_s when increasing the doping level from the non-superconducting parent compounds to optimally doped superconducting compounds. Here, in the $BaFe_{1.9-x}Ni_{0.1}Cr_xAs_2$ system, both T_N and T_s are actually within the range 32 ~ 35 K for all probed dopings [73], but the onset temperature of δ_ρ still extends to high temperatures, and it is then strongly suppressed by Cr doping (**Figure 3A**). In those hole-type compounds, δ_ρ shows a peak feature (for $x = 0.5$ and 0.6) or a kink (for $x = 0.7$ and 0.8) responding to the magnetic and structural transitions (**Figure 3B**). The non-monotonic behavior of δ_ρ may come from the competition between the scattering from hole bands and electron bands, and similar behaviors were observed in the nematic susceptiblity of the Cr doped $BaFe_2(As_{1-x}P_x)_2$ system [27].

Next, we focus on the electronic structure and the spin excitations in two typical dopings $x = 0.05$ with $T_N = 32$ K and $x = 0.5$ with $T_N = 35$ K. The Fermi surface topology and band structure measured by ARPES on naturally twinned samples are shown in **Figure 4**. From the Fermi surface mapping in **Figure 4A,B**, we can find typical hole pockets

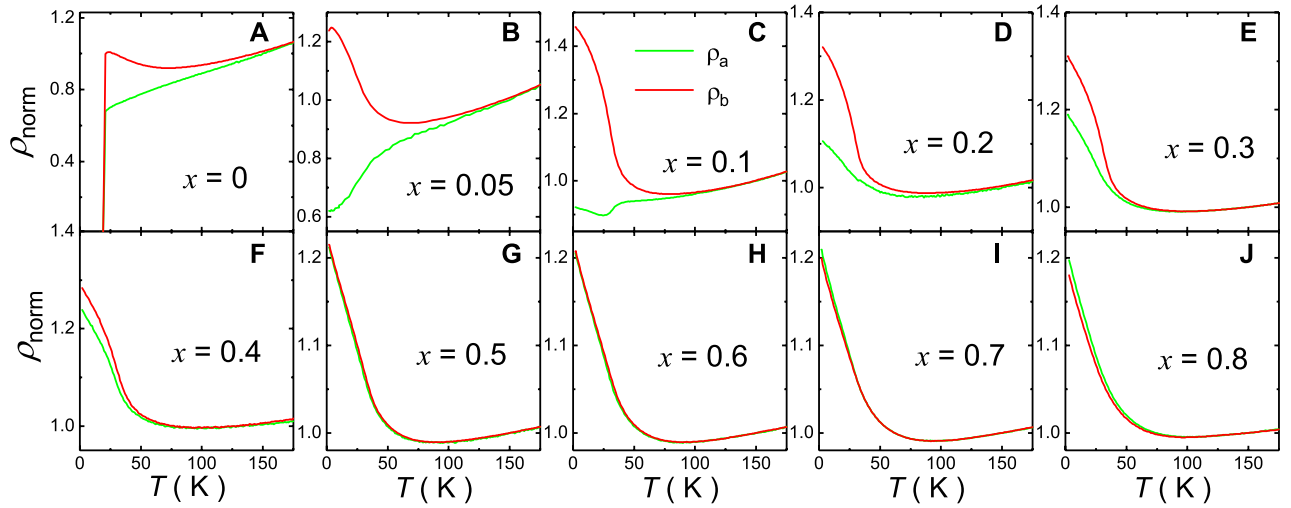

FIGURE 2 | (Color online) In-plane resistivity anisotropy of $BaFe_{1.9-x}Ni_{0.1}Cr_xAs_2$ under uniaxial pressure. Here, ρ_b is the in-plane resistivity along the direction of uniaxial pressure, and ρ_a is the in-plane resistivity perpendicular to the direction of uniaxial pressure. For easy comparison, each curve is normalized by its resistivity at 150 K, and there is no resistivity anisotropy above this temperature.

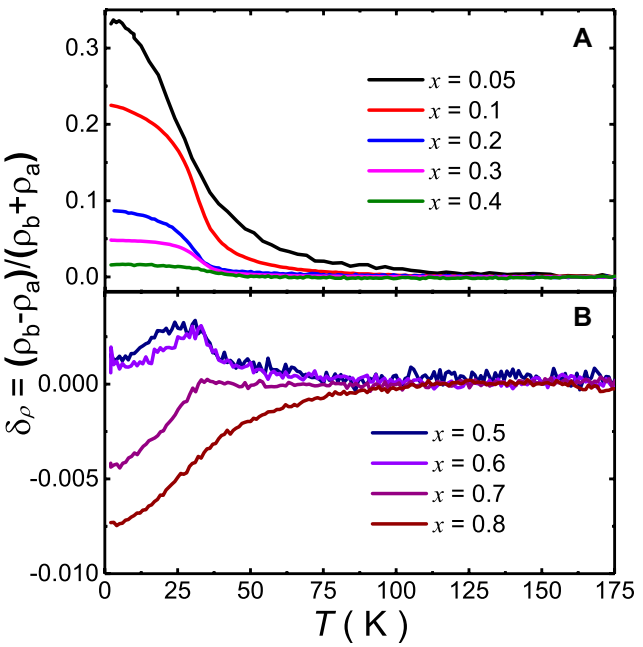

FIGURE 3 | (Color online) Temperature dependence of the in-plane resistivity anisotropy δ_ρ from $x = 0.05$ to 0.8. **(A)** In electron-type compounds, δ_ρ gets weaker but keeps positive when increasing Cr doping. **(B)** In hole-type compounds, δ_ρ is very weak and becomes negative when $x \geq 0.7$.

around the zone center Γ point. Near the X point, an electron pocket is observed for $x = 0.05$. For $x = 0.5$, however, the Fermi surface resembles that of the hole-doped $(Ba,K)Fe_2As_2$ [53]. This is due to the hole doping introduced by the Cr substitution, which also introduces disorder directly in the Fe-planes, thus resulting in spectral features that appear broad [82]. **Figure 4C,D** show the second energy derivatives of the spectral images along the high symmetry direction (Γ-X). Larger hole pockets can indeed be seen for $x = 0.5$ compared to $x = 0.05$. As has been demonstrated previously on $BaFe_2As_2$, NaFeAs, and FeSe, the onset of T_s is associated with the onset of an observed anisotropic shift of the d_{xz} and d_{yz} orbital-dominated bands where the d_{xz} band shifts down and the d_{yz} band shifts up [52–56]. This shift is most prominently observed near the X point of the Brillouin zone. Moreover, such band splitting as measured on uniaxially strained crystals can be observed above T_s in the presence of this symmetry-breaking field. On a structurally twinned crystal, the anisotropic band shifts would appear in the form of a band splitting due to domain mixing. While we do not observe clearly the band splitting as shown in **Figure 4C,D**, we can clearly observe the lower branch with dominant intensity that shifts with temperature. This can be understood as the lower d_{xz} band. We can fit the energy position of the band extracted from the X point and plot as a function of temperature. The temperature evolution clearly identifies a temperature scale associated with an onset of the band shift [53–55]. As shown in **Figure 4E,F**, the X band shifts at low temperature $T \approx 25$ K for $x = 0.05$ and $T \approx 45$ K for $x = 0.5$, respectively, closing to their structural or magnetic transition temperatures. We do note that while we cannot conclusively state that this represents the orbital anisotropy, the behavior we observe here on these twinned crystals is consistent with the expectation of the onset of orbital anisotropy [52, 57, 62]. We note here that the observed onset temperature of band splitting is close to the T_s (or T_N), in contrast to the much higher onset in the resistivity anisotropy shown in **Figure 3** measured on a strained crystal.

We then turn to search the connection between the resistivity anisotropy and the spin excitation anisotropy. The first evidence of spin nematicity was observed in $BaFe_{2-x}Ni_xAs_2$ ($x = 0$, 0.065, 0.085, 0.10, 0.12) [60–63], where $BaFe_{1.9}Ni_{0.1}As_2$

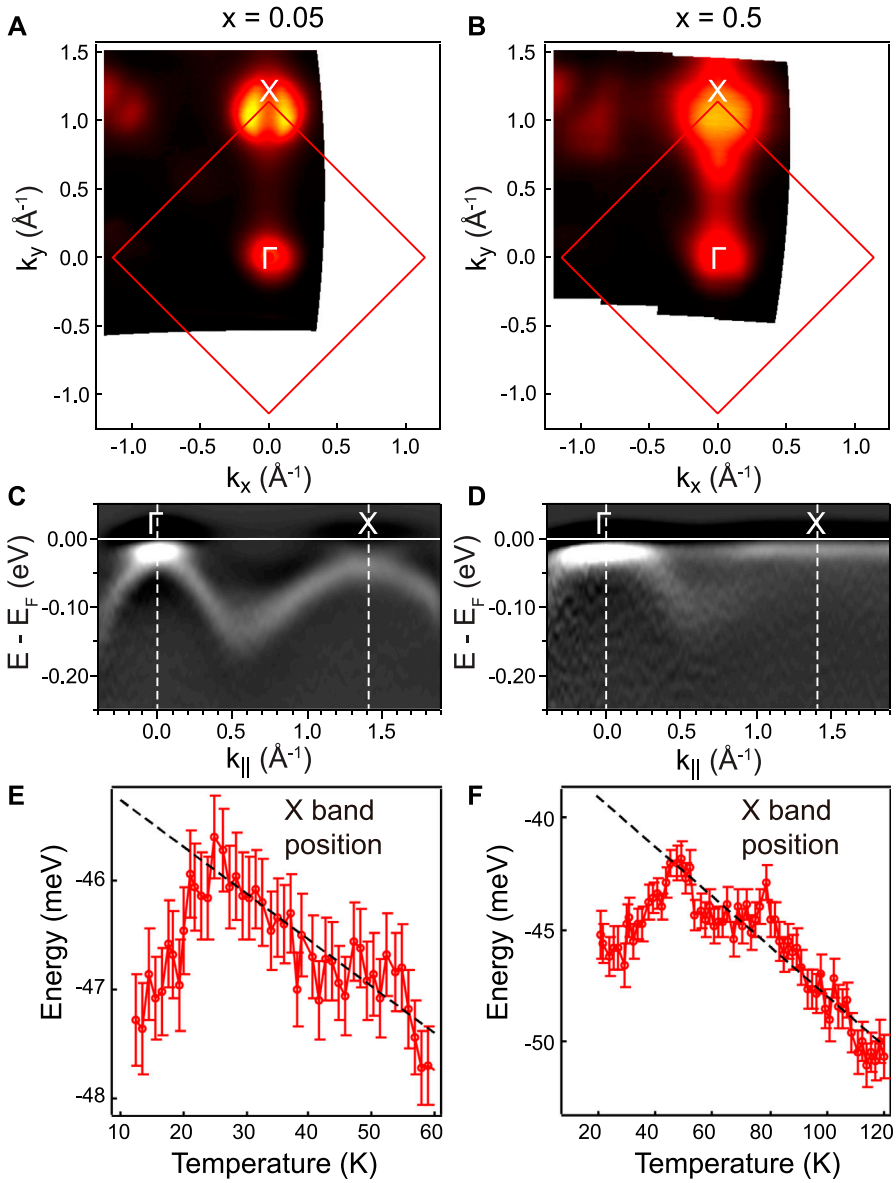

FIGURE 4 | (Color online) ARPES results on $x = 0.05$ (left) and $x = 0.5$ (right) compounds. **(A)–(B)** The measured Fermi surfaces around the Γ and X points. **(C)–(D)** Band dispersions along the high symmetry direction Γ-X obtained from the second derivatives in the energy direction. **(E)–(F)** Temperature dependence of the fitted band position from the X point. All dashed lines are guides for eyes.

is the starting compound of this study. Low-energy spin excitations are measured on the detwinned $BaFe_{1.9-x}Ni_{0.1}Cr_xAs_2$ (x = 0.05 and 0.5) samples by INS experiments using two triple-axis spectrometers. The results of constant-energy scans at E = 3, 6, 9, and 12 meV are summarized in **Figure 5**. With convenient design of the detwinned device and sample holder, we can easily perform constant-energy scans (Q – scans) either along the [H, 0, 1] or [0, K, 1] direction after rotating the whole sample set by 90°. For the x = 0.5 sample, we instead do the $S1$ rocking scans at Q = (1, 0, 1) and (0, 1, 1). It should be noticed that the Néel temperature T_N is slightly enhanced by the applied uniaxial pressure in the x = 0.05 sample from 32 to 40 K (so does T_s) but does not change for the x = 0.5 sample ($T_N \approx T_N' = 35$ K) (**Figure 6A,B**). Such an effect has been detected in the $BaFe_{2-x}(Ni, Co)_xAs_2$ system [110]. The detwinned ratio can be estimated by comparing the integrated intensities of magnetic Bragg peak between Q = (1, 0, 1) and Q = (0, 1, 1) positions, which is about 10:1 for the x = 0.05 samples, and 4:1 for the x = 0.5 samples, respectively. Such a large ratio means successful detwin for both sample sets. At the first glance, it is very clear for the difference of the spin excitations between Q = (1, 0, 1) and Q = (0, 1, 1) especially at low temperatures, which could be attributed to the spin Ising-nematic correlations (so-called spin nematicity).

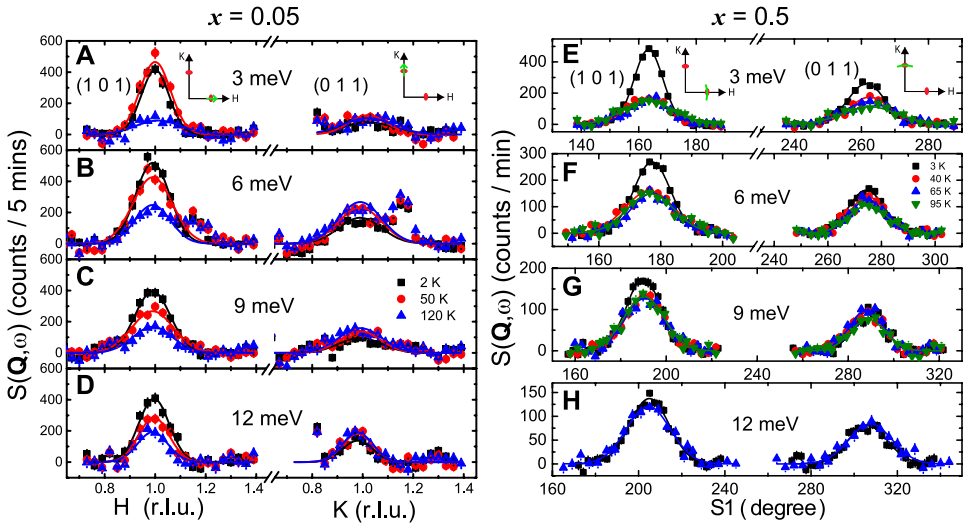

FIGURE 5 | (Color online) Inelastic neutron scattering results on the spin excitations of uniaxially detwinned samples for $x = 0.05$ (left) and $x = 0.5$ (right) compounds measured by two triple-axis spectrometers TAIPAN and PUMA. We compared the constant-energy scans (Q –scans along [H,0,1] or [0, K,1], $S1$ rocking scans at Q = (1,0,1) or (0, 1, 1)) for E = 3, 6, 9, 12 meV, respectively. All data are corrected by a linearly Q –dependent background, and the solid lines are Gaussian fittings. The spurious signals in 6 meV data are ignored.

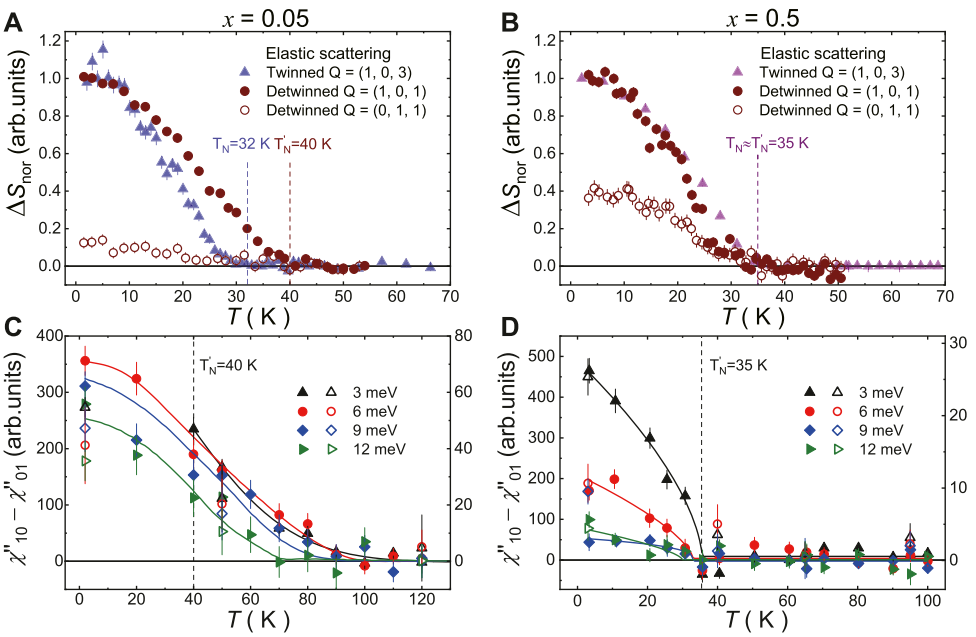

FIGURE 6 | (Color online) The order parameter of antiferromagnetism and spin nematicity $\chi''_{10} - \chi''_{01}$ for $x = 0.05$ and x =0.5 compounds. **(A)** and **(B)** The magnetic order parameters measured at Q = (1,0,3) on twinned samples, Q = (1,0,1) and Q = (0,1,1) on detwinned samples by elastic neutron scattering. All data are subtracted by the normal state background and normalized by the intensity at base temperature for Q = (1,0,3) or Q = (1,0,1). **(C)** and **(D)** Spin nematicity measured by inelastic neutron scattering. The solid symbols are the differences of local susceptibility χ'' between Q = (1,0,1) and Q = (0,1,1) (left y-axis), and the open symbols are similar but obtained by integrating the constant-energy scans in **Figure 5** corrected by the Bose population factor (right y-axis). The vertical dash lines mark the magnetic transition temperature T_N on twinned samples and T_N' on detwinned samples. All solid lines are guides to eyes.

After warming up to high temperatures, the spin excitations at Q = (1, 0, 1) decrease and become nearly identical to those at Q = (0, 1, 1). The nematic order parameter for the spin system can be approximately represented by $\chi''_{nematic} = \chi''_{10} - \chi''_{01}$, in which χ''_{10} (or χ''_{01}) is the local spin susceptibility at Q = (1, 0, 1) (or Q = (0, 1, 1)). **Figure 6C,D** show the temperature

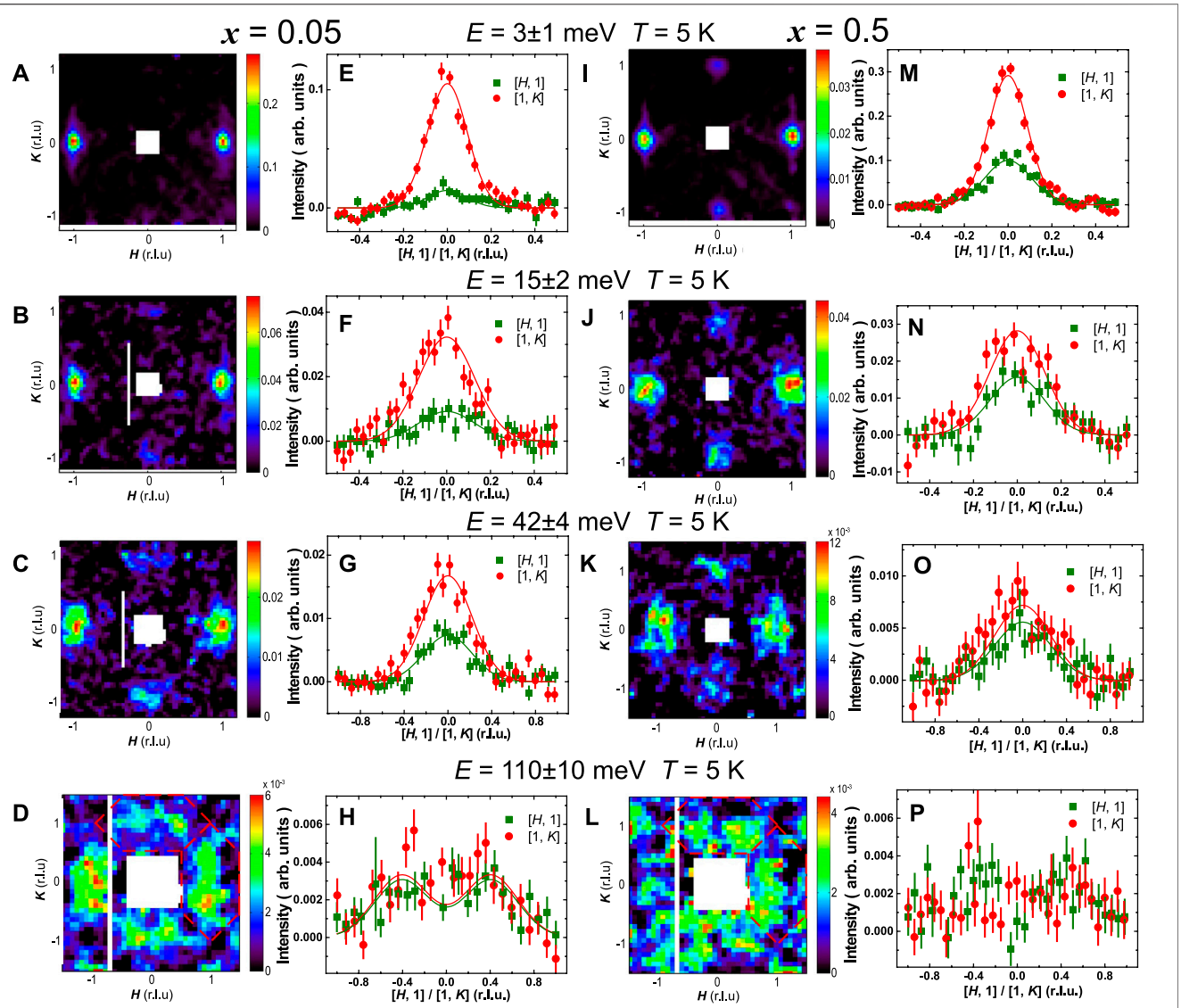

FIGURE 7 | (Color online) Inelastic neutron scattering results on the spin excitations of the uniaxially detwinned samples for x = 0.05 (left) and x = 0.5 (right) compounds measured at T = 5 K by time-of-flight spectrometer 4SEASONS. All data are presented in both 2D slices for the [H, K] plane and 1D cuts along [H,0] or [0, K] at typical energy windows E = 3±1,15±2,42±4,110±10 meV. The solid lines are Gaussian fittings guiding for eyes, which are not shown in panel **(P)** due to poor data quality. The dashed diamonds in panel **(D)** and **(L)** illustrate the integrated Brillouin zone for spin excitations around Q = (1,0) and Q = (0,1), respectively.

dependence of $\chi''_{10} - \chi''_{01}$ for both compounds, where the Bose population factor is already corrected. We also plot the data (open symbols) obtained from the integrated intensity of those Q − scans in **Figure 5**. For the x = 0.05 compound, the spin nematicity decreases slightly upon increasing energy and terminates well above T'_N = 40 K (**Figure 6C**)[73]. For the lowest energy we measured (3 meV), the onset temperature of spin nematicity is about 110 K, similar to the in-plane resistivity anisotropy in **Figure 3A**. The results for x = 0.5 compound show markedly differences, where $\chi''_{10} - \chi''_{01}$ quickly decreases with both energy and temperature, and the onset temperature is around T'_N = 35 K (**Figure 6D**). No spin anisotropy can be detected above 40 K for both Q − scans and energy scans, and this is also consistent with the very weak in-plane resistivity anisotropy for x = 0.5 (**Figure 3B**). The spin nematic theory predicts that the nematic fluctuations enhance both the intensity and the correlation length of spin excitations at (π, 0) but suppress those at (0, π) even above T_s. This was firstly testified in the detwinned $BaFe_{1.935}Ni_{0.065}As_2$ and can also be seen here in **Figure 5**[61]. Although the peak intensities at Q = (1, 0, 1) seem stronger than those at Q = (0, 1, 1) in **Figure 5G,H**, the peak width is smaller, and the integrated intensity of the Q-scans are closed to each other. The above results of spin nematicity in $BaFe_{1.9-x}Ni_{0.1}Cr_xAs_2$ (x = 0.05 and 0.5) resemble to those in $BaFe_{2-x}Ni_xAs_2$, where spin excitations at low energies change from C_4 to C_2 symmetry in the tetragonal

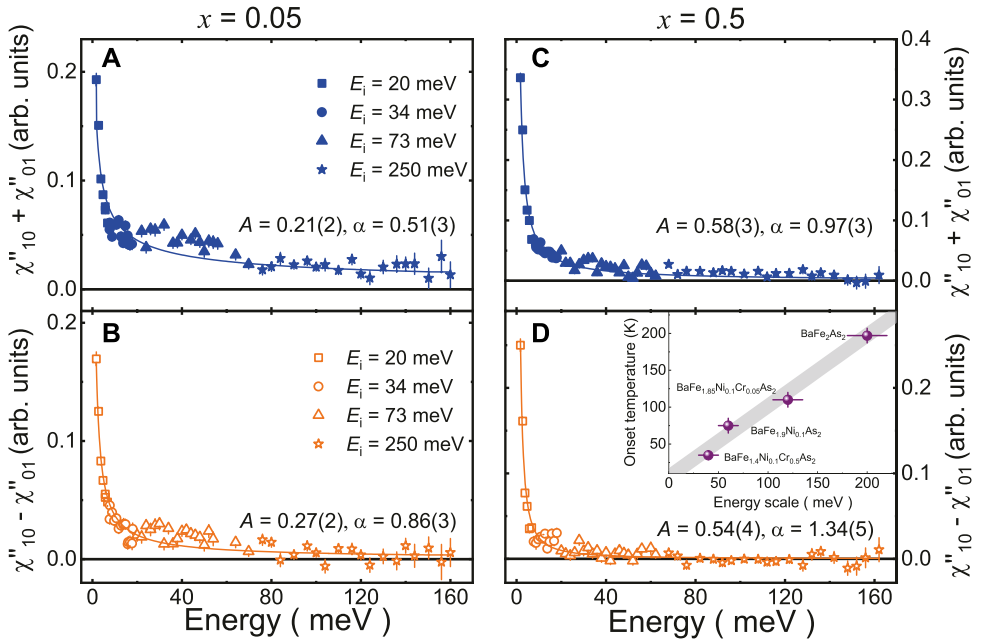

FIGURE 8 | (Color online) Energy dependence of the total spin fluctuations $\chi''_{10} + \chi''_{01}$ and the spin nematicity $\chi''_{10} - \chi''_{01}$ of uniaxially detwinned samples for x =0.05 (left) and x =0.5 (right) compounds. Different symbols correspond to different incident energies in the measurements. Both of $\chi''_{10} + \chi''_{01}$ and $\chi''_{10} - \chi''_{01}$ can be fitted with a power-law dependence on the energy, ~ A/E^{α}, where the amplitude A and exponent α are listed in each panel. The inset of panel **(D)** shows the correlation between the highest energy and the onset temperature at low energy of $\chi''_{10} - \chi''_{01}$.

phase at temperatures approximately corresponding to the onset of the in-plane resistivity anisotropy.

Moreover, INS experiments on detwinned $BaFe_2As_2$ and $BaFe_{1.9}Ni_{0.1}As_2$ suggest that the spin anisotropy can persist to very high energy [62, 63], even in the later case the splitting of the d_{xz} and d_{yz} bands nearly vanishes [57]. To quantitatively determine the energy dependence of spin excitation anisotropy, we have performed time-of-flight INS experiments on the uniaxially detwinned $BaFe_{1.9-x}Ni_{0.1}Cr_xAs_2$ (x = 0.05 and 0.5), and the results are shown in **Figures 7**, **8**. It should be noted that for such experiments, the energy transfer is always coupled with L due to $k_i \parallel c$ [102, 103]. The two-dimensional (2D) energy slices and one-dimensional (1D) cuts along [H, 0] and [0, K] at various energies are presented in **Figure 7**. Indeed, the spin excitations are twofold symmetric below 100 meV for both compounds. The spin excitations at E = 3 meV, Q = (0, ±1) are very weak in the x = 0.05 compound, then continuously increase upon energy, and become nearly the same as Q = (±1, 0) around 110 meV. For the x = 0.5 compound, although the spin excitations at Q = (0, ±1) can be initially observed at E = 3 meV, the spin anisotropy still exists at 15 meV and then disappears above 42 meV. To further compare the spin excitations in both compounds, we have calculated the total spin fluctuations $\chi''_{10} + \chi''_{01}$ and the spin nematicity $\chi''_{10} - \chi''_{01}$ from the integrated intensity marked by the dashed diamonds in **Figure 7D,L**. In principle, the local dynamic susceptibility χ' can be estimated from the integration outcome of the spin excitations within one Brillouin zone, and here χ' can be simply calculated through dividing the integration signal in the Q = (0, 0) (1, 1), (2, 0), (1, −1) boxes, giving the diamond shape integration zone [8]. The total spin susceptibility $\chi''_{10} + \chi''_{01}$ in the x = 0.5 compound is stronger than that in x = 0.05 but decays much quickly with energy (**Figure 8A,C**). The spin nematicity $\chi''_{10} - \chi''_{01}$ apparently has different energy scales for two compounds, where it is about 120 meV for x = 0.05 but only 40 meV for x = 0.5, respectively. The energy scale of $\chi''_{10} - \chi''_{01}$ in the superconducting compound $BaFe_{1.9}Ni_{0.1}As_2$ is 60 meV [62], and for the parent compound $BaFe_2As_2$, it is about 200 meV up to the band top of the spin waves [63]. These facts lead to a possible linear correlation between the highest energy and the onset temperature of spin nematicity at low energy (inset of **Figure 8D**). Within the measured energy range, both $\chi''_{10} + \chi''_{01}$ and $\chi''_{10} - \chi''_{01}$ can be fit with a power-law dependence on the energy, ~ A/E^{α}, where the amplitude A and exponent α are listed in each panel of **Figure 8**. Indeed, the larger value of α for x = 0.5 in comparison to that for x = 0.05 suggests faster decay with energy for both the spin fluctuations and the spin nematicity. Similar fitting on the results of $BaFe_{1.9}Ni_{0.1}As_2$ gives parameters in between them [62]. Although the low energy data below 10 meV may be affected by the L-modulation of spin excitations, and by the superconductivity in $BaFe_{1.9}Ni_{0.1}As_2$, the similar quantum critical behavior both for $\chi''_{10} + \chi''_{01}$ and $\chi''_{10} - \chi''_{01}$ in these three compounds is expected by the Ising-nematic scenario [60–63].

In our previous neutron diffraction results on the $BaFe_{1.9-x}Ni_{0.1}Cr_xAs_2$ system, the Cr dopings have limited effects on the magnetically ordered temperature T_N but significantly enhance the effective ordered moment m by reaching a maximum value at x = 0.5 [73]. The Néel temperature T_N is mostly determined by the local magnetic coupling related to the local $FeAs_4$ tetrahedron structure. The evolution of ordered moment probably induced by the changes of the density of states and the orbital angular momentum from itinerant electrons on the Fermi surfaces. The Cr doping

introduces both local distortion on the lattices and hole doping on the Fermi pockets, yielding a non-monotonic change of the conductivity of charge carriers. As shown in **Figure 2**, the low-temperature upturn of resistivity is enhanced by Cr doping first but then weakens in those hole-type compounds. Among these dopings, $x = 0.5$ has the most insulating-like behavior, and thus strongly localized charge carriers and maximum ordered moment, but its spin nematicity quickly drops down for both the temperature and energy dependence. In contrast to the magnetically ordered strength, both the structural transition temperature T_s and the lattice orthorhombicity $\delta = (a - b)/(a + b)$ are nearly Cr doping independent [73]. This means the static nematic order is also nearly Cr independent in this system, as opposed to the case for dynamic nematic fluctuations.

The nature of the iron-based superconductor can be theoretically described as a magnetic Hund's metal, in which the strong interplay between the local spins on Fe atoms and the itinerant electrons on Fermi surfaces gives correlated electronic states [80, 81]. Indeed, time-of-flight INS experiments on the detwinned $BaFe_2As_2$ suggest that the spin waves in the parent compound are preferably described by a multi-orbital Hubbard–Hund model based on the itinerant picture with moderate electronic correlation effects, instead of a Heisenberg model with effective exchange couplings from local spins. Upon warming up to high temperatures, the intensities of spin excitation anisotropy decrease gradually with increasing energy and finally cut off at an energy away from the band top of spin waves [63]. Therefore, the energy scale of spin nematicity sets an upper limit for the characteristic temperature for the nematic spin correlations, as well as the onset temperature of resistivity anisotropy. Here, by adding up the results on the in-plane anisotropies of resistivity, orbital energy, and spin excitations in $BaFe_{1.9-x}Ni_{0.1}Cr_xAs_2$, they clearly suggest that the electronic nematicity is intimately related to the spin dynamics, which seems consistent with Hund's metal picture. Specifically, by doping Cr to suppress the superconductivity in $BaFe_{1.9}Ni_{0.1}As_2$, it makes the charge carriers initially localized with enhanced electron correlations [73], which may enhance the electronic correlations by increasing the intra- and inter-orbital onsite repulsion U as well as Hund's coupling J_H [63], and thus gives rise to stronger spin excitations and larger spin anisotropy in the Cr doping $x = 0.05$ compound. Another effect is the lifting up of d_{yz} and d_{xy} along the Γ-X direction to the Fermi level, which primarily contributes to the effective moments [80]. The orbital-weight redistribution triggered by the spin order suggests that the orbital degree of freedom is coupled to the spin degree of freedom [111]. By further increasing Cr doping to $x = 0.5$, the localization effect is so strong that the electron system becomes insulating at low temperature. In this case, the itinerant picture based on Hund's metal may not be applicable anymore. The low density of itinerant electrons weakens the nematic fluctuations and probably limits them inside the magnetically ordered state. In either case for $x = 0.05$ or $x = 0.5$, the band splitting does not directly correspond to the spin nematic correlations but only present below the nematic ordered temperature. This may attribute to the weak spin–orbit coupling in this system, as the spin anisotropy in spin space can only present at very low energies [59]. In addition, our results can rule out the picture of local impurity scattering driven nematicity since the impurity scattering from Cr substitutions is certainly stronger in the $x = 0.5$ compound, but it does not promote the nematic fluctuations.

4 CONCLUSION

In conclusion, we have extensively studied the in-plane resistivity anisotropy, orbital ordering, and spin nematicity in a non-superconducting $BaFe_{1.9-x}Ni_{0.1}Cr_xAs_2$ system. We have found that the Cr doping strongly affect the anisotropy of resistivity and spin excitations along with the itinerancy of charge carriers. While the onset temperatures of resistivity anisotropy and spin nematicity are similar and correlated with the energy scale of spin anisotropy, the orbital anisotropy shows an onset temperature irrelevant to them. These results suggest that the electronic correlations from the interplay between local moments and itinerant electrons are crucial to understand the nematic fluctuations, thus inspiring the quest for the driven force of the electronic nematic phase in iron-pnictide superconductors.

DATA AVAILABILITY STATEMENT

The datasets presented in this article are not readily available because the datasets are currently private. Requests to access the datasets should be directed to HL, hqluo@iphy.ac.cn.

AUTHOR CONTRIBUTIONS

HL and DG proposed and designed the research. DG, TX, WZ, and RZ contributed in sample growth and resistivity measurements. MY, MW, S-KM, MH, DL, and RB contributed to the ARPES measurements. DG and HL carried out the neutron scattering experiments with SD, GD, XL, JP, KI, and KK. DG, HL, SL, and PD analyzed the data. HL, DG, and MY wrote the paper. All authors participated in discussion and comment on the paper.

FUNDING

This work is supported by the National Key Research and Development Program of China (Grant No. 2018YFA0704200, No. 2017YFA0303100, and No. 2017YFA0302900), the National Natural Science Foundation of China (Grants No. 11822411, No. 11961160699, and No. 12061130200), the Strategic Priority Research Program (B) of the CAS (Grant No. XDB25000000 and No. XDB07020300), and the KC Wong Education Foundation (GJTD-2020-01). HL is grateful for the support from the Youth Innovation Promotion Association of CAS (Grant No. Y202001) and the Beijing Natural Science Foundation (Grant No. JQ19002). MW is supported by the National Natural Science Foundation of China (Grant No. 11904414 and No.12174454), the Guangdong Basic and Applied Basic Research Foundation (No. 2021B1515120015), and the National Key Research and Development Program of China (No. 2019YFA0705702). The work at University of California, Berkeley, and Lawrence Berkeley National Laboratory was funded by the U.S. Department of Energy (DOE), Office of Science, Office of Basic Energy Sciences, Materials Sciences and Engineering Division under Contract No. DE-AC02-05-CH11231 within the Quantum Materials Program (KC2202) and

the Office of Basic Energy Sciences. The ARPES work at Rice University was supported by the Robert A. Welch Foundation (Grant No. C-2024 (MY)). The neutron scattering work at Rice University was supported by the U.S. DOE, BES (Grant No. DE-SC0012311) and by the Robert A. Welch Foundation (Grant No. C-1839 (PD)).

ACKNOWLEDGMENTS

The authors thank the helpful discussion with Xingye Lu at Beijing Normal University and Yu Song at Zhejiang University. The neutron scattering experiments in this work are performed at thermal triple-axis spectrometer PUMA at Heinz Maier-Leibnitz Zentrum (MLZ), Germany, thermal triple-axis spectrometer TAIPAN at Australian Centre for Neutron Scattering (ACNS), Australian Nuclear Science and Technology Organisation (ANSTO), Australia (Proposal No. P4263), and time-of-flight Fermi-chopper spectrometer 4SEASONS (BL-01) at the Materials and Life Science Experimental Facility of J-PARC (Proposal Nos. 2015A0005, 2016A0169). ARPES measurements were performed at the Advanced Light Source and the Stanford Radiation Lightsource, which are both operated by the Office of Basic Energy Sciences, U.S. DOE.

REFERENCES

1. Oganesyan V, Kivelson SA, Fradkin E. Quantum Theory of a Nematic Fermi Fluid. *Phys Rev B* (2001) 64:195109. doi:10.1103/physrevb.64.195109
2. Fradkin E, Kivelson SA. Electron Nematic Phases Proliferate. *Science* (2010) 327:155–6. doi:10.1126/science.1183464
3. Fradkin E, Kivelson SA, Lawler MJ, Eisenstein JP, Mackenzie AP. Nematic Fermi Fluids in Condensed Matter Physics. *Annu Rev Condens Matter Phys* (2010) 1:153–78. doi:10.1146/annurev-conmatphys-070909-103925
4. Wang W, Luo J, Wang C, Yang J, Kodama Y, Zhou R, et al. Microscopic Evidence for the Intra-unit-cell Electronic Nematicity inside the Pseudogap Phase in $YBa_2Cu_4O_8$. *Sci China Phys Mech Astron* (2021) 64:237413. doi:10.1007/s11433-020-1615-y
5. Fernandes RM, Schmalian J. Manifestations of Nematic Degrees of Freedom in the Magnetic, Elastic, and Superconducting Properties of the Iron Pnictides. *Supercond Sci Technol* (2012) 25:084005. doi:10.1088/0953-2048/25/8/084005
6. Fernandes RM, Chubukov AV. Low-energy Microscopic Models for Iron-Based Superconductors: a Review. *Rep Prog Phys* (2017) 80:014503. doi:10.1088/1361-6633/80/1/014503
7. Chen X, Dai P, Feng D, Xiang T, Zhang F-C. Iron-based High Transition Temperature Superconductors. *Nat Sci Rev* (2014) 1:371–95. doi:10.1093/nsr/nwu007
8. Dai P. Antiferromagnetic Order and Spin Dynamics in Iron-Based Superconductors. *Rev Mod Phys* (2015) 87:855–96. doi:10.1103/revmodphys.87.855
9. Si Q, Yu R, Abrahams E. High-temperature Superconductivity in Iron Pnictides and Chalcogenides. *Nat Rev Mat* (2016) 1:16017. doi:10.1038/natrevmats.2016.17
10. Gong Dong-Liang D, Luo Hui-Qian H. Antiferromagnetic Order and Spin Dynamics in Iron-Based Superconductors. *Acta Phys Sin* (2018) 67:207407. doi:10.7498/aps.67.20181543
11. Böhmer AE, Meingast C. Electronic Nematic Susceptibility of Iron-Based Superconductors. *Comptes Rendus Phys* (2016) 17:90–112. doi:10.1016/j.crhy.2015.07.001
12. Chu J-H, Kuo H-H, Analytis JG, Fisher IR. Divergent Nematic Susceptibility in an Iron Arsenide Superconductor. *Science* (2012) 337:710–2. doi:10.1126/science.1221713
13. Kuo H-H, Fisher IR. Effect of Disorder on the Resistivity Anisotropy Near the Electronic Nematic Phase Transition in Pure and Electron-Doped $BaFe_2As_2$. *Phys Rev Lett* (2014) 112:227001. doi:10.1103/physrevlett.112.227001
14. Kuo H-H, Shapiro MC, Riggs SC, Fisher IR. Measurement of the Elastoresistivity Coefficients of the Underdoped Iron Arsenide $Ba(Fe_{0.975}Co_{0.025})_2As_2$. *Phys Rev B* (2013) 88:085113. doi:10.1103/physrevb.88.085113
15. Böhmer AE, Burger P, Hardy F, Wolf T, Schweiss P, Fromknecht R, et al. Nematic Susceptibility of Hole-Doped and Electron-Doped $BaFe_2As_2$ Iron-Based Superconductors from Shear Modulus Measurements. *Phys Rev Lett* (2014) 112:047001. doi:10.1103/PhysRevLett.112.047001
16. Gong D, Liu Z, Gu Y, Xie T, Ma X, Luo H, et al. Nature of the Antiferromagnetic and Nematic Transitions in $Sr_{1-x}Ba_xFe_{1.97}Ni_{0.03}As_2$. *Phys Rev B* (2017) 96:104514. doi:10.1103/physrevb.96.104514
17. Böhmer AE, Chen F, Meier WR, Xu M, Drachuck G, Merz M, et al. Evolution of Nematic Fluctuations in $CaK(Fe_{1-x}Ni_x)_4As_4$ with Spin-Vortex Crystal Magnetic Order [Preprint] (2020). Available at: https://arxiv.org/abs/2011.13207.
18. Kuo H-H, Chu J-H, Palmstrom JC, Kivelson SA, Fisher IR. Ubiquitous Signatures of Nematic Quantum Criticality in Optimally Doped Fe-Based Superconductors. *Science* (2016) 352:958–62. doi:10.1126/science.aab0103
19. Yoshizawa M, Kimura D, Chiba T, Simayi S, Nakanishi Y, Kihou K, et al. Structural Quantum Criticality and Superconductivity in Iron-Based Superconductor $Ba(Fe_{1-x}Co_x)_2As_2$. *J Phys Soc Jpn* (2012) 81:024604. doi:10.1143/jpsj.81.024604
20. Dai J, Si Q, Zhu J-X, Abrahams E. Iron Pnictides as a New Setting for Quantum Criticality. *Proc Natl Acad Sci USA* (2009) 106:4118–21. doi:10.1073/pnas.0900886106
21. Kasahara S, Shi HJ, Hashimoto K, Tonegawa S, Mizukami Y, Shibauchi T, et al. Electronic Nematicity above the Structural and Superconducting Transition in $BaFe_2(As_{1-x}P_x)_2$. *Nature* (2012) 486:382–5. doi:10.1038/nature11178
22. Shibauchi T, Carrington A, Matsuda Y. A Quantum Critical Point Lying beneath the Superconducting Dome in Iron Pnictides. *Annu Rev Condens Matter Phys* (2014) 5:113–35. doi:10.1146/annurev-conmatphys-031113-133921
23. Lederer S, Schattner Y, Berg E, Kivelson SA. Superconductivity and Non-fermi Liquid Behavior Near a Nematic Quantum Critical Point. *Proc Natl Acad Sci USA* (2015) 114:4905–10. doi:10.1073/pnas.1620651114
24. Luo H, Zhang R, Laver M, Yamani Z, Wang M, Lu X, et al. Coexistence and Competition of the Short-Range Incommensurate Antiferromagnetic Order with the Superconducting State of $BaFe_{2-x}Ni_xAs_2$. *Phys Rev Lett* (2012) 108:247002. doi:10.1103/physrevlett.108.247002
25. Lu X, Gretarsson H, Zhang R, Liu X, Luo H, Tian W, et al. Avoided Quantum Criticality and Magnetoelastic Coupling in $BaFe_{2-x}Ni_xAs_2$. *Phys Rev Lett* (2013) 110:257001. doi:10.1103/physrevlett.110.257001
26. Hu D, Lu X, Zhang W, Luo H, Li S, Wang P, et al. Structural and Magnetic Phase Transitions Near Optimal Superconductivity in $BaFe_2(As_{1-x}P_x)_2$. *Phys Rev Lett* (2015) 114:157002. doi:10.1103/physrevlett.114.157002
27. Zhang W, Wei Y, Xie T, Liu Z, Gong D, Ma X, et al. Unconventional Antiferromagnetic Quantum Critical Point in $Ba(Fe_{0.97}Cr_{0.03})_2(As_{1-x}P_x)_2$. *Phys Rev Lett* (2019) 122:037001. doi:10.1103/physrevlett.122.037001
28. Liu Z, Gu Y, Zhang W, Gong D, Zhang W, Xie T, et al. Nematic Quantum Critical Fluctuations in $BaFe_{2-x}Ni_xAs_2$. *Phys Rev Lett* (2016) 117:157002. doi:10.1103/physrevlett.117.157002
29. Gu Y, Liu Z, Xie T, Zhang W, Gong D, Hu D, et al. Unified Phase Diagram for Iron-Based Superconductors. *Phys Rev Lett* (2017) 119:157001. doi:10.1103/physrevlett.119.157001
30. Chandra P, Coleman P, Larkin AI. Ising Transition in Frustrated Heisenberg Models. *Phys Rev Lett* (1990) 64:88–91. doi:10.1103/physrevlett.64.88
31. Hu J, Xu C. Nematic Orders in Iron-Based Superconductors. *Phys C Supercond* (2012) 481:215–22. doi:10.1016/j.physc.2012.05.002
32. Fernandes RM, Chubukov AV, Schmalian J. What Drives Nematic Order in Iron-Based Superconductors? *Nat Phys* (2014) 10:97–104. doi:10.1038/nphys2877
33. Fernandes RM, Chubukov AV, Knolle J, Eremin I, Schmalian J. Preemptive Nematic Order, Pseudogap, and Orbital Order in the Iron Pnictides. *Phys Rev B* (2012) 85:024534. doi:10.1103/physrevb.85.024534
34. Wang F, Kivelson SA, Lee D-H. Nematicity and Quantum Paramagnetism in FeSe. *Nat Phys* (2015) 11:959–63. doi:10.1038/nphys3456

35. Ma C, Wu L, Yin W-G, Yang H, Shi H, Wang Z, et al. Strong Coupling of the Iron-Quadrupole and Anion-Dipole Polarizations in $Ba(Fe_{1-x}Co_x)_2As_2$. *Phys Rev Lett* (2014) 112:077001. doi:10.1103/physrevlett.112.077001
36. Thorsmølle VK, Khodas M, Yin ZP, Zhang C, Carr SV, Dai P, et al. Critical Quadrupole Fluctuations and Collective Modes in Iron Pnictide Superconductors. *Phys Rev B* (2016) 93:054515. doi:10.1103/physrevb.93.054515
37. Wang Q, Shen Y, Pan B, Hao Y, Ma M, Zhou F, et al. Strong Interplay between Stripe Spin Fluctuations, Nematicity and Superconductivity in FeSe. *Nat Mater* (2015) 15:159–63. doi:10.1038/nmat4492
38. Chubukov AV, Fernandes RM, Schmalian J. Origin of Nematic Order in FeSe. *Phys Rev B* (2015) 91:201105(R). doi:10.1103/physrevb.91.201105
39. Yamakawa Y, Onari S, Kontani H. Nematicity and Magnetism in FeSe and Other Families of F-Based Superconductors. *Phys Rev X* (2016) 6:021032. doi:10.1103/physrevx.6.021032
40. Lee C-C, Yin W-G, Ku W. Ferro-Orbital Order and Strong Magnetic Anisotropy in the Parent Compounds of Iron-Pnictide Superconductors. *Phys Rev Lett* (2009) 103:267001. doi:10.1103/physrevlett.103.267001
41. Krüger F, Kumar S, Zaanen J, van den Brink J. Spin-orbital Frustrations and Anomalous Metallic State in Iron-Pnictide Superconductors. *Phys Rev B* (2009) 79:054504. doi:10.1103/physrevb.79.054504
42. Lv W, Wu J, Phillips P. Orbital Ordering Induces Structural Phase Transition and the Resistivity Anomaly in Iron Pnictides. *Phys Rev B* (2009) 80:224506. doi:10.1103/physrevb.80.224506
43. Chen C-C, Maciejko J, Sorini AP, Moritz B, Singh RRP, Devereaux TP. Orbital Order and Spontaneous Orthorhombicity in Iron Pnictides. *Phys Rev B* (2010) 82:100504(R). doi:10.1103/physrevb.82.100504
44. Valenzuela B, Bascones E, Calderón MJ. Conductivity Anisotropy in the Antiferromagnetic State of Iron Pnictides. *Phys Rev Lett* (2010) 105:207202. doi:10.1103/physrevlett.105.207202
45. Chu J-H, Analytis JG, De Greve K, McMahon PL, Islam Z, Yamamoto Y, et al. In-Plane Resistivity Anisotropy in an Underdoped Iron Arsenide Superconductor. *Science* (2010) 329:824–6. doi:10.1126/science.1190482
46. Tanatar MA, Blomberg EC, Kreyssig A, Kim MG, Ni N, Thaler A, et al. Uniaxial-strain Mechanical Detwinning of $CaFe_2As_2$ and $BaFe_2As_2$ Crystals: Optical and Transport Study. *Phys Rev B* (2010) 81:184508. doi:10.1103/physrevb.81.184508
47. Ying JJ, Wang XF, Wu T, Xiang ZJ, Liu RH, Yan YJ, et al. Measurements of the Anisotropic In-Plane Resistivity of Underdoped FeAs-Based Pnictide Superconductors. *Phys Rev Lett* (2011) 107:067001. doi:10.1103/PhysRevLett.107.067001
48. Man H, Lu X, Chen JS, Zhang R, Zhang W, Luo H, et al. Electronic Nematic Correlations in the Stress-free Tetragonal State of $BaFe_{2-x}Ni_xAs_2$. *Phys Rev B* (2015) 92:134521. doi:10.1103/physrevb.92.134521
49. Luo X, Stanev V, Shen B, Fang L, Ling XS, Osborn R, et al. Antiferromagnetic and Nematic Phase Transitions in $BaFe_2(As_{1-x}P_x)_2$ Studied by Ac Microcalorimetry and SQUID Magnetometry. *Phys Rev B* (2015) 91:094512. doi:10.1103/physrevb.91.094512
50. Mirri C, Dusza A, Bastelberger S, Chu J-H, Kuo H-H, Fisher IR, et al. Hysteretic Behavior in the Optical Response of the Underdoped Fe Arsenide $Ba(Fe_{1-x}Co_x)_2As_2$ in the Electronic Nematic Phase. *Phys Rev B* (2014) 89:060501(R). doi:10.1103/physrevb.89.060501
51. Fisher IR, Degiorgi L, Shen ZX. In-plane Electronic Anisotropy of Underdoped '122' Fe-Arsenide Superconductors Revealed by Measurements of Detwinned Single Crystals. *Rep Prog Phys* (2011) 74:124506. doi:10.1088/0034-4885/74/12/124506
52. Yi M, Lu D, Chu J-H, Analytis JG, Sorini AP, Kemper AF, et al. Symmetry-breaking Orbital Anisotropy Observed for Detwinned $Ba(Fe_{1-x}Co_x)_2$ as 2 above the Spin Density Wave Transition. *Proc Natl Acad Sci USA* (2011) 108:6878–83. doi:10.1073/pnas.1015572108
53. Yi M, Zhang Y, Liu Z-K, Ding X, Chu J-H, Kemper AF, et al. Dynamic Competition between Spin-Density Wave Order and Superconductivity in Underdoped $Ba_{1-x}K_xFe_2As_2$. *Nat Commun* (2014) 5:3711. doi:10.1038/ncomms4711
54. Yi M, Lu DH, Moore RG, Kihou K, Lee C-H, Iyo A, et al. Electronic Reconstruction through the Structural and Magnetic Transitions in Detwinned NaFeAs. *New J Phys* (2012) 14:073019. doi:10.1088/1367-2630/14/7/073019
55. Yi M, Pfau H, Zhang Y, He Y, Wu H, Chen T, et al. Nematic Energy Scale and the Missing Electron Pocket in FeSe. *Phys Rev X* (2019) 9:041049. doi:10.1103/physrevx.9.041049
56. Zhang Y, He C, Ye ZR, Jiang J, Chen F, Xu M, et al. Symmetry Breaking via Orbital-dependent Reconstruction of Electronic Structure in Detwinned NaFeAs. *Phys Rev B* (2012) 85:085121. doi:10.1103/physrevb.85.085121
57. Yi M, Zhang Y, Shen Z-X, Lu D. Role of the Orbital Degree of Freedom in Iron-Based Superconductors. *npj Quant Mater* (2017) 2:57. doi:10.1038/s41535-017-0059-y
58. Watson MD, Dudin P, Rhodes LC, Evtushinsky DV, Iwasawa H, Aswartham S, et al. Probing the Reconstructed Fermi Surface of Antiferromagnetic $BaFe_2As_2$ in One Domain. *npj Quantum Mat* (2019) 4:36. doi:10.1038/s41535-019-0174-z
59. Luo H, Wang M, Zhang C, Lu X, Regnault L-P, Zhang R, et al. Spin Excitation Anisotropy as a Probe of Orbital Ordering in the Paramagnetic Tetragonal Phase of Superconducting $BaFe_{1.904}Ni_{0.096}As_2$. *Phys Rev Lett* (2013) 111:107006. doi:10.1103/physrevlett.111.107006
60. Lu X, Park JT, Zhang R, Luo H, Nevidomskyy AH, Si Q, et al. Nematic Spin Correlations in the Tetragonal State of Uniaxial-Strained $BaFe_{2-x}Ni_x$ as 2. *Science* (2014) 345:657–60. doi:10.1126/science.1251853
61. Zhang W, Park JT, Lu X, Wei Y, Ma X, Hao L, et al. Effect of Nematic Order on the Low-Energy Spin Fluctuations in Detwinned $BaFe_{1.935}Ni_{0.065}As_2$. *Phys Rev Lett* (2016) 117:227003. doi:10.1103/physrevlett.117.227003
62. Song Y, Lu X, Abernathy DL, Tam DW, Niedziela JL, Tian W, et al. Energy Dependence of the Spin Excitation Anisotropy in Uniaxial-Strained $BaFe_{1.9}Ni_{0.1}As_2$. *Phys Rev B* (2015) 92:180504(R). doi:10.1103/physrevb.92.180504
63. Lu X, Scherer DD, Tam DW, Zhang W, Zhang R, Luo H, et al. Spin Waves in Detwinned $BaFe_2As_2$. *Phys Rev Lett* (2018) 121:067002. doi:10.1103/physrevlett.121.067002
64. Ren X, Duan L, Hu Y, Li J, Zhang R, Luo H, et al. Nematic Crossover in $BaFe_2As_2$ under Uniaxial Stress. *Phys Rev Lett* (2015) 115:197002. doi:10.1103/physrevlett.115.197002
65. Hu Y, Ren X, Zhang R, Luo H, Kasahara S, Watashige T, et al. Nematic Magnetoelastic Effect Contrasted between $Ba(Fe_{1-x}Co_x)_2As_2$ and FeSe. *Phys Rev B* (2016) 93:060504(R). doi:10.1103/physrevb.93.060504
66. Baek S-H, Efremov DV, Ok JM, Kim JS, van den Brink J, Büchner B. Orbital-driven Nematicity in FeSe. *Nat Mater* (2015) 14:210–4. doi:10.1038/nmat4138
67. Iye T, Julien M-H, Mayaffre H, Horvatić M, Berthier C, Ishida K, et al. Emergence of Orbital Nematicity in the Tetragonal Phase of $BaFe_2(As_{1-x}P_x)_2$. *J Phys Soc Jpn* (2015) 84:043705. doi:10.7566/jpsj.84.043705
68. Rosenthal EP, Andrade EF, Arguello CJ, Fernandes RM, Xing LY, Wang XC, et al. Visualization of Electron Nematicity and Unidirectional Antiferroic Fluctuations at High Temperatures in NaFeAs. *Nat Phys* (2014) 10:225–32. doi:10.1038/nphys2870
69. Ishida S, Nakajima M, Liang T, Kihou K, Lee CH, Iyo A, et al. Anisotropy of the In-Plane Resistivity of Underdoped $Ba(Fe_{1-x}Co_x)_2As_2$ Superconductors Induced by Impurity Scattering in the Antiferromagnetic Orthorhombic Phase. *Phys Rev Lett* (2013) 110:207001. doi:10.1103/physrevlett.110.207001
70. Allan MP, Chuang T-M, Massee F, Xie Y, Ni N, Bud'ko SL, et al. Anisotropic Impurity States, Quasiparticle Scattering and Nematic Transport in Underdoped $Ca(Fe_{1-x}Co_x)_2As_2$. *Nat Phys* (2013) 9:220–4. doi:10.1038/nphys2544
71. Zhang R, Gong D, Lu X, Li S, Dai P, Luo H. The Effect of Cr Impurity to Superconductivity in Electron-Doped $BaFe_{2-x}Ni_xAs_2$. *Supercond Sci Technol* (2014) 27:115003. doi:10.1088/0953-2048/27/11/115003
72. Zhang R, Gong D, Lu X, Li S, Laver M, Niedermayer C, et al. Doping Evolution of Antiferromagnetism and Transport Properties in Nonsuperconducting $BaFe_{2-2x}Ni_xCr_xAs_2$. *Phys Rev B* (2015) 91:094506. doi:10.1103/physrevb.91.094506
73. Gong D, Xie T, Zhang R, Birk J, Niedermayer C, Han F, et al. Doping Effects of Cr on the Physical Properties of $BaFe_{1.9-x}Ni_{0.1}Cr_xAs_2$. *Phys Rev B* (2018) 98:014512. doi:10.1103/physrevb.98.014512
74. Pizarro JM, Calderón MJ, Liu J, Muñoz MC, Bascones E. Strong Correlations and the Search for High-T_c Superconductivity in Chromium Pnictides and Chalcogenides. *Phys Rev B* (2017) 95:075115. doi:10.1103/physrevb.95.075115

75. Edelmann M, Sangiovanni G, Capone M, de' Medici L. Chromium Analogs of Iron-Based Superconductors. *Phys Rev B* (2017) 95:205118. doi:10.1103/physrevb.95.205118
76. de'Medici L, Giovannetti G, Capone M. Selective Mott Physics as a Key to Iron Superconductors. *Phys Rev Lett* (2014) 112:177001. doi:10.1103/physrevlett.112.177001
77. Lee PA, Nagaosa N, Wen X-G. Doping a Mott Insulator: Physics of High-Temperature Superconductivity. *Rev Mod Phys* (2006) 78:17–85. doi:10.1103/revmodphys.78.17
78. Gu Q, Wen H-H. Superconductivity in Nickel-Based 112 Systems. *The Innovation* (2022) 3:100202. doi:10.1016/j.xinn.2021.100202
79. Song Y, Yamani Z, Cao C, Li Y, Zhang C, Chen JS, et al. A Mott Insulator Continuously Connected to Iron Pnictide Superconductors. *Nat Commun* (2016) 7:13879. doi:10.1038/ncomms13879
80. Yin ZP, Haule K, Kotliar G. Kinetic Frustration and the Nature of the Magnetic and Paramagnetic States in Iron Pnictides and Iron Chalcogenides. *Nat Mater* (2011) 10:932–5. doi:10.1038/nmat3120
81. Georges A, Medici Ld., Mravlje J. Strong Correlations from Hund's Coupling. *Annu Rev Condens Matter Phys* (2013) 4:137–78. doi:10.1146/annurev-conmatphys-020911-125045
82. Yi M, Lu DH, Analytis JG, Chu J-H, Mo S-K, He R-H, et al. Electronic Structure of the $BaFe_2As_2$ Family of Iron-Pnictide Superconductors. *Phys Rev B* (2009) 80:024515. doi:10.1103/physrevb.80.024515
83. Richard P, Sato T, Nakayama K, Takahashi T, Ding H. Fe-based Superconductors: an Angle-Resolved Photoemission Spectroscopy Perspective. *Rep Prog Phys* (2011) 74:124512. doi:10.1088/0034-4885/74/12/124512
84. Song Y, Wang W, Zhang C, Gu Y, Lu X, Tan G, et al. Temperature and Polarization Dependence of Low-Energy Magnetic Fluctuations in Nearly Optimally Doped $NaFe_{0.9785}Co_{0.0215}As$. *Phys Rev B* (2017) 96:184512. doi:10.1103/physrevb.96.184512
85. Song Y, Man H, Zhang R, Lu X, Zhang C, Wang M, et al. Spin Anisotropy Due to Spin-Orbit Coupling in Optimally Hole-Doped $Ba_{0.67}K_{0.33}Fe_2As_2$. *Phys Rev B* (2016) 94:214516. doi:10.1103/physrevb.94.214516
86. Xie T, Wei Y, Gong D, Fennell T, Stuhr U, Kajimoto R, et al. Odd and Even Modes of Neutron Spin Resonance in the Bilayer Iron-Based Superconductor $CaKFe_4As_4$. *Phys Rev Lett* (2018) 120:267003. doi:10.1103/physrevlett.120.267003
87. Xie T, Gong D, Ghosh H, Ghosh A, Soda M, Masuda T, et al. Neutron Spin Resonance in the 112-Type Iron-Based Superconductor. *Phys Rev Lett* (2018) 120:137001. doi:10.1103/physrevlett.120.137001
88. Xie T, Liu C, Bourdarot F, Regnault L-P, Li S, Luo H. Spin-excitation Anisotropy in the Bilayer Iron-Based Superconductor $CaKFe_4As_4$. *Phys Rev Res* (2020) 2:022018(R). doi:10.1103/physrevresearch.2.022018
89. Wang T, Zhang C, Xu L, Wang J, Jiang S, Zhu Z, et al. Strong Pauli Paramagnetic Effect in the Upper Critical Field of $KCa_2Fe_4As_4F_2$. *Sci China Phys Mech Astron* (2020) 63:227412. doi:10.1007/s11433-019-1441-4
90. Guo J, Yue L, Iida K, Kamazawa K, Chen L, Han T, et al. Preferred Magnetic Excitations in the Iron-Based $Sr_{1-x}Na_xFe_2As_2$ Superconductor. *Phys Rev Lett* (2019) 122:017001. doi:10.1103/physrevlett.122.017001
91. Liu C, Bourges P, Sidis Y, Xie T, He G, Bourdarot F, et al. Preferred Spin Excitations in the Bilayer Iron-Based Superconductor $CaK(Fe_{0.96}Ni_{0.04})_4As_4$ with Spin-Vortex Crystal Order. *Phys Rev Lett* (2022) 128:137003. doi:10.1103/physrevlett.128.137003
92. Luo H, Wang Z, Yang H, Cheng P, Zhu X, Wen H-H. Growth and Characterization of $A_{1-x}K_xFe_2As_2$(A = Ba, Sr) Single Crystals With x= 0-0.4. *Supercond Sci Technol* (2008) 21:125014. doi:10.1088/0953-2048/21/12/125014
93. Chen Y, Lu X, Wang M, Luo H, Li S. Systematic Growth of $BaFe_{2-x}Ni_xAs_2$ Large Crystals. *Supercond Sci Technol* (2011) 24:065004. doi:10.1088/0953-2048/24/6/065004
94. Xie T, Gong D, Zhang W, Gu Y, Huesges Z, Chen D, et al. Crystal Growth and Phase Diagram of 112-type Iron Pnictide Superconductor $Ca_{1-y}La_yFe_{1-x}Ni_xAs_2$. *Supercond Sci Technol* (2017) 30:095002. doi:10.1088/1361-6668/aa7994
95. Wang T, Chu J, Feng J, Wang L, Xu X, Li W, et al. Low Temperature Specific Heat of 12442-type $KCa_2Fe_4As_4F_2$ Single Crystals. *Sci China Phys Mech Astron* (2020) 63:297412. doi:10.1007/s11433-020-1549-9
96. Lu X, Tseng K-F, Keller T, Zhang W, Hu D, Song Y, et al. Impact of Uniaxial Pressure on Structural and Magnetic Phase Transitions in Electron-Doped Iron Pnictides. *Phys Rev B* (2016) 93:134519. doi:10.1103/physrevb.93.134519
97. Tam DW, Wang W, Zhang L, Song Y, Zhang R, Carr SV, et al. Weaker Nematic Phase Connected to the First Order Antiferromagnetic Phase Transition in $SrFe_2As_2$ Compared to $BaFe_2As_2$. *Phys Rev B* (2019) 99:134519. doi:10.1103/physrevb.99.134519
98. Tam DW, Yin ZP, Xie Y, Wang W, Stone MB, Adroja DT, et al. Orbital Selective Spin Waves in Detwinned NaFeAs. *Phys Rev B* (2020) 102:054430. doi:10.1103/physrevb.102.054430
99. Liu P, Klemm ML, Tian L, Lu X, Song Y, Tam DW, et al. In-plane Uniaxial Pressure-Induced Out-of-Plane Antiferromagnetic Moment and Critical Fluctuations in $BaFe_2As_2$. *Nat Commun* (2020) 11:5728. doi:10.1038/s41467-020-19421-5
100. Sobolev O, Park JT. PUMA: Thermal Three Axes Spectrometer. *J Large Scale Res Facil* (2015) 1:A13. doi:10.17815/jlsrf-1-36
101. Danilkin SA, Yethiraj M. TAIPAN: Thermal Triple-Axis Spectrometer. *Neutron News* (2009) 20:37–9. doi:10.1080/10448630903241217
102. Nakamura M, Kajimoto R, Inamura Y, Mizuno F, Fujita M, Yokoo T, et al. First Demonstration of Novel Method for Inelastic Neutron Scattering Measurement Utilizing Multiple Incident Energies. *J Phys Soc Jpn* (2009) 78:093002. doi:10.1143/jpsj.78.093002
103. Kajimoto R, Nakamura M, Inamura Y, Mizuno F, Nakajima K, Ohira-Kawamura S, et al. The Fermi Chopper Spectrometer 4SEASONS at J-PARC. *J Phys Soc Jpn* (2011) 80:SB025. doi:10.1143/jpsjs.80sb.sb025
104. Inamura Y, Nakatani T, Suzuki J, Otomo T. Development Status of Software "Utsusemi" for Chopper Spectrometers at MLF, J-PARC. *J Phys Soc Jpn* (2013) 82:SA031. doi:10.7566/jpsjs.82sa.sa031
105. ISIS Facility. *ISIS Facility, Rutherford Appleton Laboratory, UK* (2000). Available at: https://www.isis.stfc.ac.uk/Pages/Excitations-Software.aspx.
106. Blomberg EC, Tanatar MA, Fernandes RM, MazinII, Shen B, Wen H-H, et al. Sign-reversal of the In-Plane Resistivity Anisotropy in Hole-Doped Iron Pnictides. *Nat Commun* (2013) 4:1914. doi:10.1038/ncomms2933
107. Ma JQ, Luo XG, Cheng P, Zhu N, Liu DY, Chen F, et al. Evolution of Anisotropic In-Plane Resistivity with Doping Level in $Ca_{1-x}Na_xFe_2As_2$ Single Crystals. *Phys Rev B* (2014) 89:174512. doi:10.1103/physrevb.89.174512
108. Kobayashi T, Tanaka K, Miyasaka S, Tajima S. Importance of Fermi Surface Topology for In-Plane Resistivity Anisotropy in Hole- and Electron-Doped $Ba(Fe_{1-x}TM_x)_2As_2$ (TM = Cr, Mn, and Co). *J Phys Soc Jpn* (2015) 84:094707. doi:10.7566/jpsj.84.094707
109. Ishida K, Tsujii M, Hosoi S, Mizukami Y, Ishida S, Iyo A, et al. Novel Electronic Nematicity in Heavily Hole-Doped Iron Pnictide Superconductors. *Proc Natl Acad Sci USA* (2020) 117:6424–9. doi:10.1073/pnas.1909172117
110. Tam DW. Uniaxial Pressure Effect on the Magnetic Ordered Moment and Transition Temperatures in $BaFe_{2-x}T_xAs_2$ (T = Co, Ni). *Phys Rev B* (2017) 95:060505(R). doi:10.1103/physrevb.95.060505
111. Daghofer M, Luo Q-L, Yu R, Yao DX, Moreo A, Dagotto E. Orbital-weight Redistribution Triggered by Spin Order in the Pnictides. *Phys Rev B* (2010) 81:180514(R). doi:10.1103/physrevb.81.180514

Conflict of Interest: The authors declare that the research was conducted in the absence of any commercial or financial relationships that could be construed as a potential conflict of interest.